P1.14 ANALYSIS OF OFFSHORE DEEP CONVECTION WITHIN LANDFALLING HURRICANES JUST PRIOR TO TORNADOGENESIS

Matthew D. Eastin *
Michael C. Link
Heather B. Anderson

Department of Geography and Earth Sciences,
University of North Carolina at Charlotte, Charlotte, North Carolina

1. INTRODUCTION

The majority of landfalling tropical cyclones produce tornadoes. In the United States, as much as 10% of all deaths associated with tropical cyclones (TCs) are the result of tornadoes (Novlan and Gray 1974). To date, forecasting such TC tornado events remains a significant challenge since the typical TC environment is often very different from the typical tornadic environment.

A number of observational and numerical studies have documented common environmental and storm-scale characteristics associated with the formation of TC tornadoes (Novlan and Gray 1974; Gentry 1983; McCaul 1991; McCaul and Weisman 1996; Spratt et al. 2000; McCaul et al. 2004; Curtis 2004; Schneider and Sharp 2007). TC tornadoes predominantly form in convective outer rainbands located in the onshore flow of the right-front quadrant, usually within 100 to 400 km of the storm center. Favorable environmental characteristics include: strong low-level shear (> 20 m/s over the lowest 0-3 km), moderate CAPE (> 500 J/kg), strong low-level storm-relative helicity (> 100 m^2/s^2), dry air at midlevels adjacent to the rainband, a low-level thermal boundary or convergence axis, and small near-surface dewpoint depressions (i.e., a low LCL). Many TC tornadoes are spawned by "mini-supercells", which are shallower (echo tops $<$ 8-12 km) and smaller in diameter (< 10 km) than the classic Great Plains supercells. On radar, mini-supercells often exhibit weak hook echoes and shallow (< 5 km), small diameter (< 4 km) mesocyclones with storm-relative rotational velocities of 5-20 m/s. The mesocyclones are often short lived (< 20 min) but detectable 10-15 min prior to tornadogenesis.

Based on a review of previous studies, the current working model for TC tornadogenesis embodies a two-stage process that begins as convective cells (e.g. within an outer rainband) move onshore. During this transition from the offshore regime, enhanced surface friction increases the low-level shear and storm-relative helicity such that the local low-CAPE environment becomes favorable for the formation of mini-supercells (McCaul and Weisman 1996). Tornadogenesis is then believed to result from the tilting and subsequent stretching of this shear-generated horizontal vorticity into the vertical by buoyant updrafts (Gentry 1983). Further enhancements to the local horizontal vorticity (and the increased likelihood of tornadogenesis) can result as the cell moves over and/or interacts with pre-existing thermal boundaries, convergence zones, or outflow boundaries (generated by evaporatively-driven downdrafts). Indeed, the majority of TC mesocyclones are first observed as the cells move onshore, and many TC tornadoes are reported within 200 km of the coast during short-lived interactions with low-level boundaries.

There are also a considerable number of TC tornadoes that are reported within 10 km of the coastline. Such cases may represent an accelerated version of the conceptual model, whereby the supercell development and tornadogenesis processes simply occur over a much shorter time period (and distance) due to a very rapid increases in vertical shear and low-level convergence. However, *another possible explanation is that the mini-supercells developed well offshore.* Indeed, Bogner at al. (2000) demonstrated that the offshore TC environment is often conducive to supercell formation. Unfortunately, observations and statistics of offshore development from land-based radars are limited due to sampling considerations (Spratt et al. 2000).

The objectives of this study are to document the frequency of offshore supercell development in TC rainbands, as well as the environmental characteristics and essential physical processes involved with such development. To achieve this goal, we employ an array of land-based and airborne observations to document the three-dimensional structure and evolution of multiple convective cells embedded within offshore rainbands of landfalling tropical cyclones. Presented here are some preliminary results from an offshore rainband in Hurricane Ivan (2004). We

* *Corresponding Author Address:* Matthew D. Eastin, Department of Geography and Earth Sciences, University of North Carolina at Charlotte, 9201 University City Blvd, Charlotte, NC 28223; email: mdeastin@uncc.edu,

will demonstrate that mini-supercells were present within the rainband as far as 100 km offshore, and subsequently produced deadly tornadoes soon after moving onshore.

2. DATA AND MESOSCALE OVERVIEW

Hurricane Ivan made landfall early in the morning on 16 September 2004 just west of Gulf Shores, Alabama as a category 3 hurricane. Over 115 tornadoes were reported as Ivan crossed the southeast U.S. Eight people were killed and 17 were injured by the tornadoes. The most significant tornadic activity occurred during the afternoon and evening of 15 September as Ivan approached the Gulf coast. During this time, an intense outer rainband developed ∼200 km east of the storm center and produced multiple supercells over the Florida panhandle (see Figs. 1 and 2). This paper examines a subset of these supercells, which spawned at least 14 tornadoes that killed six and injured another 16 people.

During the afternoon and evening of 15 September, NOAA research aircraft observed Ivan's offshore environment and inner core. The two WP-3D aircraft made four penetrations of the intense outer rainband as they ferried between Ivan's eyewall and MacDill Air Force Base in Tampa, Florida. (The primary goals of the research missions were not to document the rainband, but rather the eyewall structure and evolution at landfall.) The aircraft employed the the fore-aft scanning technique (FAST) to collect dual-Doppler velocity data within the rainband during each pass (discussed in the next section). The G-IV aircraft flew around Ivan deploying multiple GPS dropwindsondes in the offshore rainband environment. Conventional satellite, rawindsonde, and the WSR-88D radar data from Tampa (TBW) and Tallahassee (TLH) were also incorporated to provide more complete depiction of the rainband environment and convective cell evolution.

Our period of interest encompasses 1500-2100 UTC on 15 September. Figure 1a shows the 89-GHz ice-scattering signature within Hurricane Ivan at 1850 UTC. The outer rainband is oriented along a south-north line and contains multiple deep convective cells (low brightness temperatures). Animated GOES-IR imagery (not shown) suggests that these cells comprise a series of convective bursts whereby cells first develop along the southern end and move northward. Figure 2 shows the base reflectivity field from the TLH radar at 1804 UTC. Multiple deep convective cells are oriented along a southeast-northwest line at regular 10-20 km intervals. Note that many cells within 20-30 km of the coastline (60-80 km from the radar) exhibit hook-like appendages indicative of supercells, but few cells at greater distances exhibit such structure. The stratiform rain shield extends to the east and northeast away from the TC center, whereas the western (inner) edge is characterized by strong reflectivity gradients and no stratiform precipitation. Figure 1b shows the GOES water vapor signature from 1825 UTC. A distinct slot of upper and midlevel dry air is located just west of the rainband.

At 1800 UTC the thermodynamic sounding from Tampa Bay (Fig. 3; ∼150 km east of the rainband) revealed a shallow moist layer near the surface (below 900 mb), drier air at midlevels (900-400 mb), and moist air aloft (above 400 mb). Conditional instability (for a surface parcel) was present through a deep layer with a CAPE of ∼2500 J/kg. The vertical wind profile exhibits modest shear (13-14 m/s) and storm-relative helicity (∼75 m^2/s^2) over the 0-3 km layer. The thermodynamic sounding from the GPS dropsonde deployed at 1807 UTC (Fig. 4; ∼40 km west of the rainband) revealed cooler and drier air near the surface, less conditional instability (CAPE ∼900 J/kg) that was restricted to mid-levels (800-400 mb), and a stable layer aloft. In contrast, the vertical wind profile exhibits strong shear (20-22 m/s) and high storm-relative helicity (∼180 m^2/s^2) over the lower levels. Both soundings support the potential for deep, rotating convection.

3. CONVECTIVE CELL STRUCTURE

Here we present the dual-Doppler observations collected between 1750 and 1815 UTC as an WP-3D aircraft was passed through the rainband at 2.5 km altitude (see the yellow box in Fig. 2). The three-dimensional wind field was constructed following the methods of Gamache (1998). During this period, the mean cell motion was at 23 m/s from the south-southeast (i.e., the cells were moving ∼10 m/s slower than the deep-layer mean wind).

Shown in Figure 5 are the radar reflectivity and storm-relative winds at 1.5 km altitude from the dual-Doppler analysis. Three distinct cells (labeled A, B, and C) are evident. Moreover, each cell contains modest cyclonic rotation in the storm-relative wind field (i.e., a mesocyclone) and a hook-like reflectivity appendage. Further examination reveals that each mesocyclone is also roughly collocated with the updraft and vertical vorticity maxima of their host cell (see Fig. 6). Clearly, each cell contains a rotating updraft: the signature of a supercell.

Figure 7 shows a north-south cross-section through the center of Cell B (see Fig. 6 for orientation). The mesocyclone (defined by the 2 x 10^{-3} s^{-1} vertical vorticity contour) extends from near the surface up to ∼4 km altitude with a diameter of ∼5-6 km. The updraft (defined by the 2 m/s vertical velocity contour) extends from ∼1.5 km upward to ∼4.5 km with a similar diameter. Such dimen-

sions are consistent with previous observations of mini-supercells within tropical cyclones (Spratt et al. 1997; McCaul et al. 2004; Schneider and Sharp 2007). Furthermore, note how the vorticity maximum ($\sim$7 x 10^{-3} s^{-1} at 1 km altitude) is located below the updraft maximum ($\sim$6 m/s at 2.5 km altitude), which suggests that vorticity stretching by the updraft may further enhance the low-level vorticity maximum. Cross-sections through Cells A and C (not shown) exhibit similar structure.

4. COASTLINE TORNADOGENESIS

Using the Tallahassee (TLH) radar, the three mini-supercells were tracked from their offshore location at $\sim$1804 UTC (see Fig. 2) until $\sim$2100 UTC, by which time each cell had moved onshore along the Florida panhandle.

From the TLH perspective, Cells A and B first exhibited a prominent hook echo when they were located $\sim$20 km offshore and $\sim$140 km from the radar. The hook echoes persisted for $\sim$30-40 minutes as the cells paralleled the coast ($\sim$5-10 km offshore and $\sim$130 km from the radar), but became less distinct as the cells moved onshore (see Fig. 8). No tornadoes nor radar-detected mesocyclones were observed in association with Cell A during this period. A weak mesocyclone was briefly detected within Cell B as it was located over a barrier island south of Panama City Beach ($<$ 5 km offshore and $\sim$125 km from the radar), but no tornadoes were reported.

Cell C first exhibited a hook echo at 1934 UTC when it was located $\sim$32 km offshore and $\sim$140 km from the radar. The hook echo persisted over the next 90 minutes as the cell paralleled the coast and then moved onshore south of Panama City Beach (Fig. 8). A weak to moderate mesocyclone was detected by the TLH radar between 2022 and 2040 UTC as the cell moved from $\sim$10 km offshore to $\sim$5 km onshore (at $\sim$120-130 km from the radar). Cell C spawned up to three tornadoes between 2040 and 2055 UTC: the most intense killed one person and injured seven others as it produced F1 damage moving through a commercial district.

5. DISCUSSION

Our preliminary results from Hurricane Ivan indicate that mini-supercells can indeed develop more than 100 km offshore within the tropical cyclone outer rainband environment. The cells exhibited many of the same structural characteristics as the mini-supercells often observed moving onshore or inland. However, the extent to which the convective structures observed within Ivan's outer rainband are typical remains an open question. Indeed, many environmental characteristics conducive to supercell formation (e.g. large CAPE, large low-level storm-relative helicity, and a midlevel dry air intrusion) were not only present, but greater in magnitude than normal (McCaul 1991; Bogner et al. 2000). Ongoing research involves documenting the environmental characteristics and convective structure of the many offshore outer rainbands for which airborne dual-Doppler radar data are available.

The early identification and regular monitoring of mini-supercells is crucial to operational forecasting. Unfortunately, the detection of mini-supercells at large ranges from land-based radars (i.e., far offshore) can be limited due to the cell's diminutive structure and radar sampling considerations (Spratt et al. 1997). For example, Cell B was located $\sim$220 km away from the Tallahassee radar when the dual-Doppler analysis was performed. At this range, the 0.5° beam would pass through the cell at $\sim$5 km altitude (see Fig. 7) and effectively overshoot the shallow mesocyclone. Thus, in an attempt to extend our ability to monitor offshore supercells, ongoing research also involves documenting the radar characteristics of numerous tornadic and non-tornadic cells as they move onshore, as well as the radar characteristics of those offshore mini-supercells identified by the airborne dual-Doppler analyses.

REFERENCES

Bogner, P. B., G. M. Barnes, and J. L. Franklin, 2000: Conditional instability and shear for six hurricanes over the Atlantic Ocean. *Wea. Forecasting*, **15**, 192-207.

Gamache, J. F., 1998: Evaluation of a fully three-dimensional variational Doppler analysis technique. Preprints, *28th Conf. on Radar Meteorology*, Austin, TX, Amer. Meteor. Soc., 422-423.

Gentry, R. C. , 1983: Genesis of tornadoes associated with hurricanes, *Mon. Wea. Rev.*, **115**, 1793-1805.

Curtis, L., 2004: Midlevel dry intrusions as a factor in tornado outbreaks associated with landfalling tropical cyclones for the Atlantic and Gulf of Mexico. *Wea. Forecasting*, **19**, 411-427.

McCaul, E. W., Jr, 1991:Buoyancy and shear characteristics of hurricane-tornado environments. *Mon. Wea. Rev.*, **119**, 1954-1978.

McCaul, E. W., Jr., D. E. Buechler, S. J. Goodman, and M. Cammarata, 2004: Doppler radar and lightning network observations of a severe outbreak of tropical cyclone tornadoes. *Mon. Wea. Rev.*, **132**, 1747-1763.

McCaul, E. W., and M. L. Weisman, 1996: Simulations of shallow supercells in landfalling hurricane environments. *Mon. Wea. Rev.*, **124**, 408-429.

Novlan, D. J., and W. M. Gray, 1974: Hurricane-spawned tornadoes. *Mon. Wea. Rev.*, **102**, 476-488.

Schneider, D., and S. Sharp, 2007: Radar signatures of tropical cyclone tornadoes in central North Carolina. *Wea. Forecasting*, **22**, 479-501.

Spratt, S. M., D. W. Sharp, P. Welsh, A. Sandrik, F. Alsheimer, and C. Paxton, 1997: A WSR-88D assessment of tropical cyclone outer rainband tornadoes. *Wea. Forecasting*, **13**, 479-501.

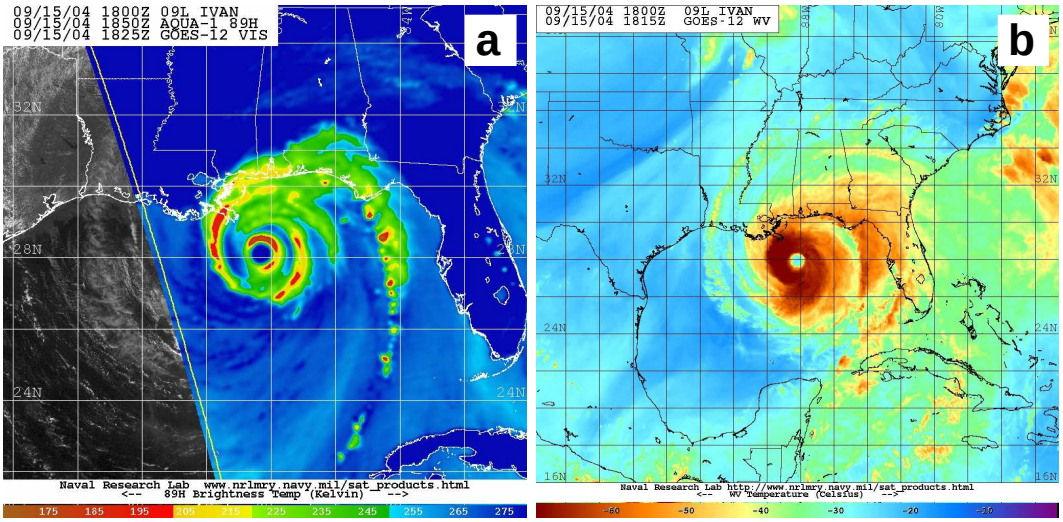

Figure 1: (a) 89-GHz brightness temperatures at 1850 UTC and (b) water vapor temperatures at 1815 UTC in Hurricane Ivan on 15 September 2004. Note the intense convective cells embedded within the outer rainband east of the storm center, as well as the dry air intrusion between the moist outer rainband and the inner core. Images from the NRL Tropical Cyclone Page.

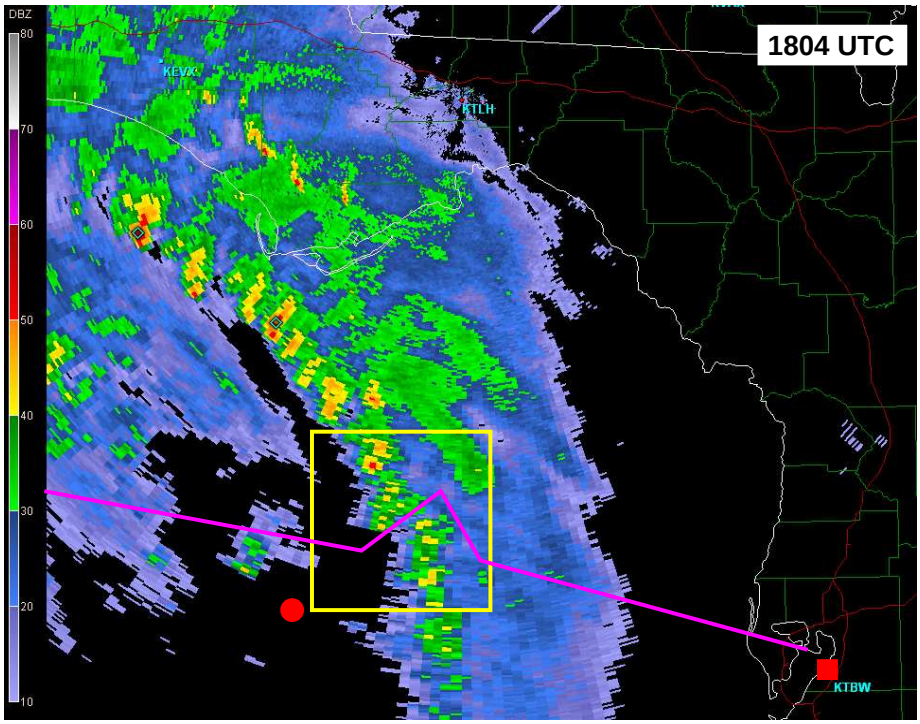

Figure 2: Base reflectivity from the Tallahassee (KTLH) WSR-88D radar at 1804 UTC on 15 September 2004. Also shown are the NOAA WP-3D flight track between 1710 and 1835 UTC (purple line), the dual-Doppler analysis region (yellow box), and the locations of the GPS sonde deployed at 1807 UTC (red circle) and the 1800 UTC Tampa Bay (KTBW) rawindsonde (red box).

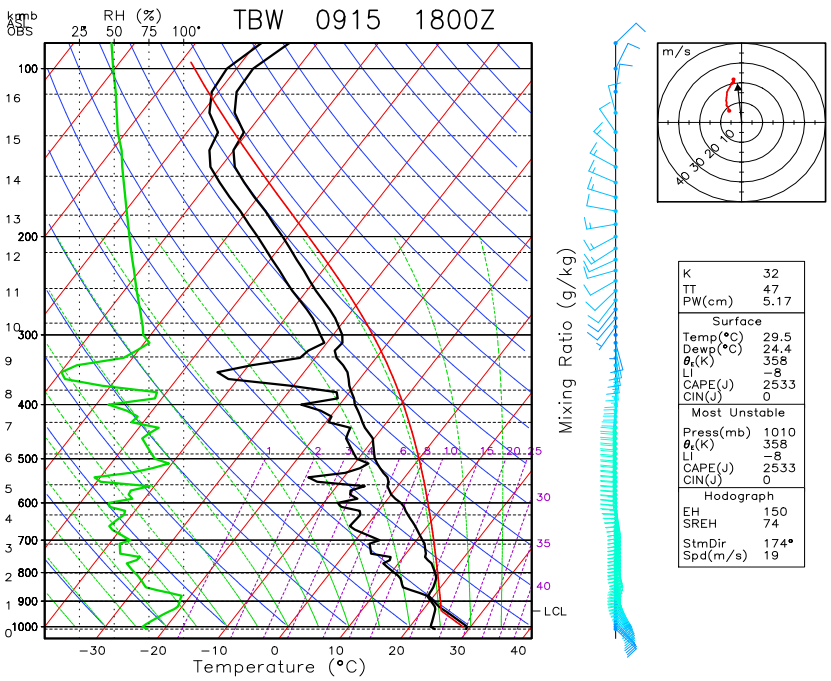

Figure 3: Skew-T plot of temperature, dewpoint, relative humidity, and winds for the Tampa sounding at 1800 UTC on 15 September 2004. Also shown is a surface-based parcel (red), the SFC-700 mb hodograph, an estimated cell motion vector (from the 900-200 mb mean wind), and a selection of standard indices.

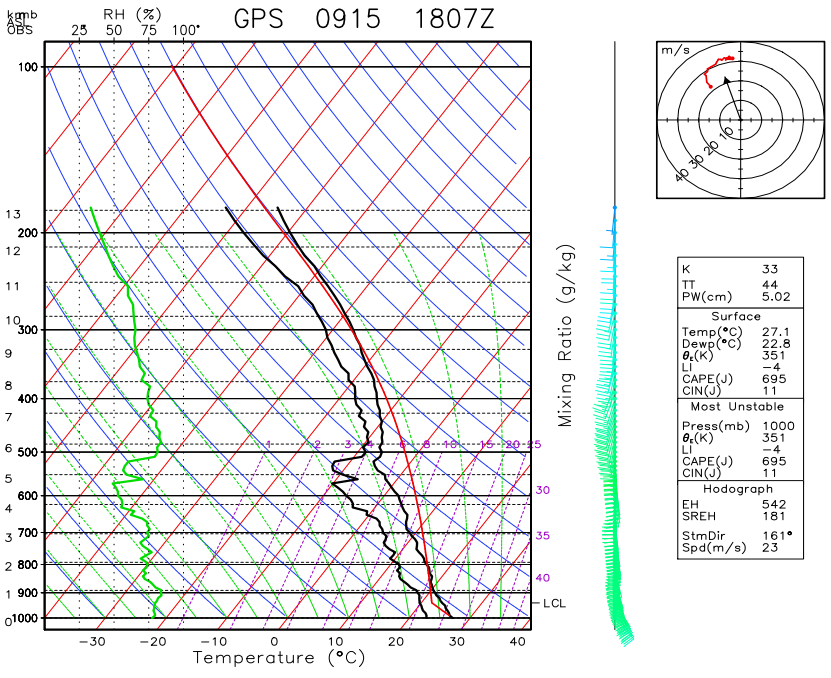

Figure 4: As in Figure 3, but for the GPS dropsonde deployed at 1807 UTC west of the rainband. The observed cell motion was used rather than an estimate from the deep layer mean wind.

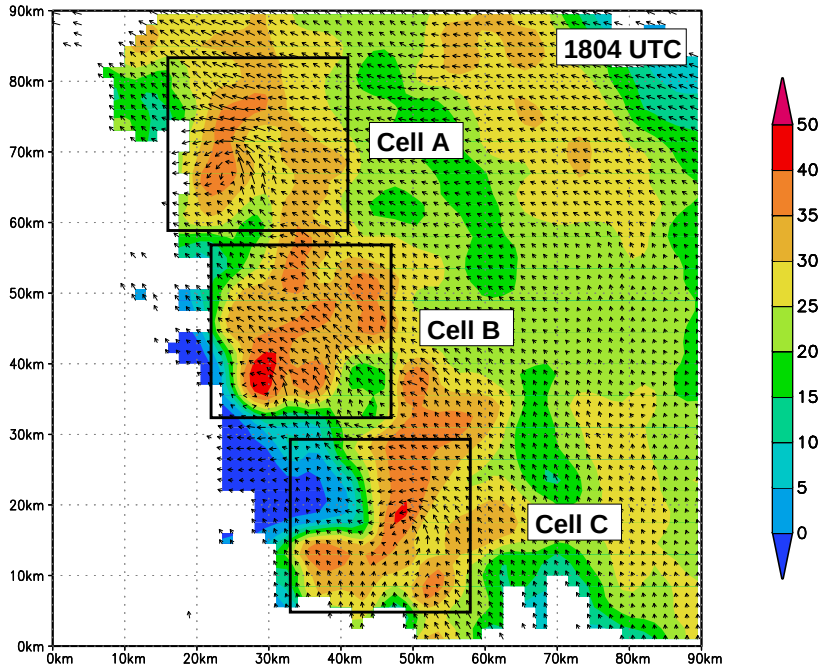

Figure 5: Radar reflectivity and dual-Doppler derived cell-relative wind vectors at 1.5 km altitude at ∼1804 UTC on 15 September 2004. Note the mesocyclonic flow associated with each cell.

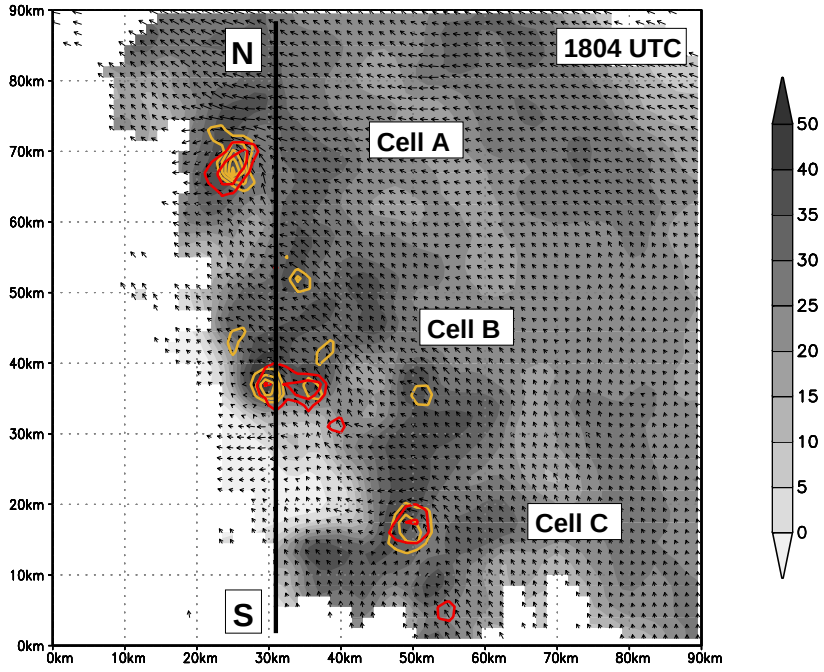

Figure 6: Radar reflectivity, vertical velocity > 2 m s^{-1} (red), vertical vorticity > 2 x 10^{-3} s^{-1} (orange), and cell-relative wind vectors at 1.5 km altitude. Note the collocated updraft and vorticity maxima; the defining signature of a rotating updraft within a supercell.

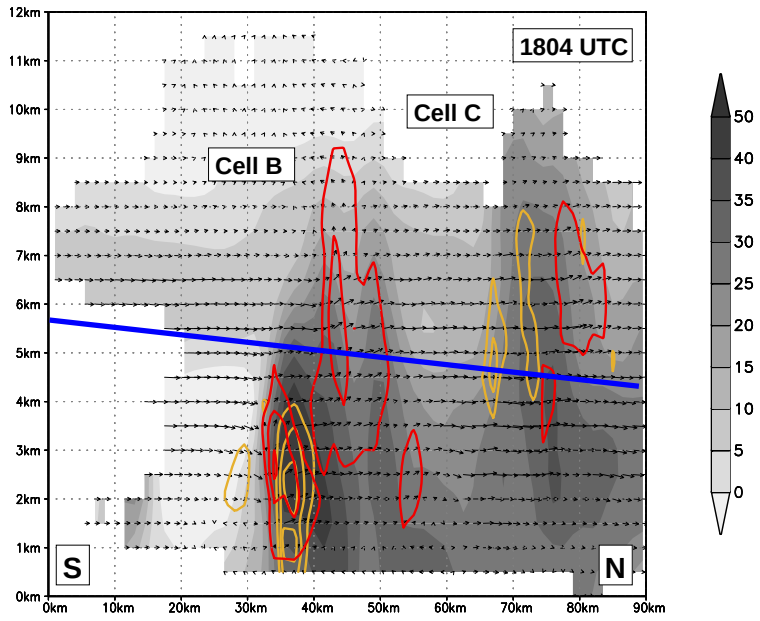

Figure 7: Radar reflectivity, vertical velocity > 2 m s^{-1} (red), vertical vorticity > 2 x 10^{-3} s^{-1} (orange), and cell-relative wind vectors along a north-south cross section through Cell B. Wind vectors depict the vertical and meridional flow. Also shown is the approximate location of the 0.5° elevation angle radar beam from the Tallahassee radar (blue line). Cell B was located ~220 km south of the radar at this time.

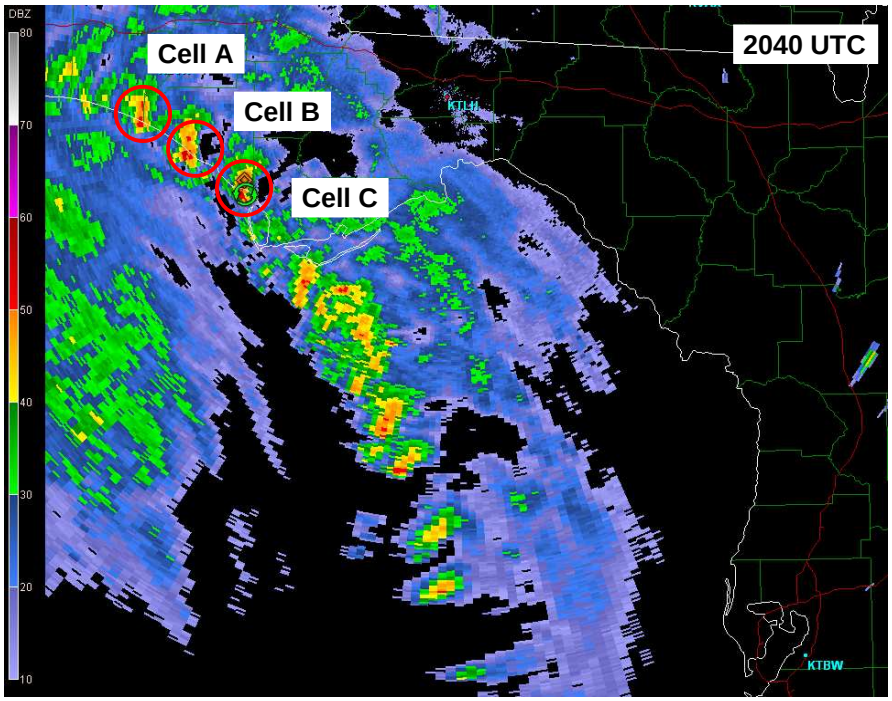

Figure 8: Base reflectivity from the Tallahassee (KTLH) radar at 2040 UTC on 15 September 2004. The locations of Cells A, B, and C are noted. Cell C has a weak radar-detected mesocyclone at this time. Over the course of the next 20 min, Cell C produced 3 tornadoes.